Comparison of the Time-reversal MUSIC and BP Algorithms in Multi-target Detection

Bing Li and Bin-Jie Hu
School of Electronic and Information Engineering
South China University of Technology, Guangzhou 510641, China

Abstract— Multi-target detection based on the time-reversal imaging with multiple signal classification (TR-MUSIC) and back-projection (BP) algorithms is presented in this paper. In the TR-MUSIC, firstly, the backscatter of a signal transmitted into a scattering environment is recorded. Secondly, the time reversal operator is obtained with the use of transfer matrix. Finally, the targets can be located through back-propagation of the eigenvectors of time reversal operator. In the BP, the imaging map is reconstructed by using the power of the electromagnetic wave corresponding to the travelling time from the transceivers to each pixel in imaging region. The imaging basic theories of TR-MUSIC and BP algorithms are outlined. In order to illustrate the performance of these two algorithms in detail, numerical simulations for three ideal point-like targets are conducted and analyzed. Here, we consider two versions of the simulation: targets detection with enough detection elements or not. Results show that the TR-MUSIC approach has a better performance than BP approach.

1. INTRODUCTION

Time-reversal imaging with multiple signal classification (TR-MUSIC) and back-projection (BP) algorithms are two well-developed imaging approaches dedicated to many applications, such as military, civil and biomedical imaging applications [1–5].

There are two stages in the time reversal process (TRP), namely, the time reversal forward propagation (TRFP) stage and the time reversal backward propagation (TRBP) stage. In the TRFP stage, the sources generate a signal, or the scatterers reflect a signal. A set of receivers record the signal. In the TRBP stage, these recorded signals are time reversed and rebroadcasted into the same scattering environment from the transmitters. The TRP is strictly within the framework of the wave equation [6]. In the contrast to the TR approach, the BP algorithm is a geometrical technique [7]. As a result, the imaging formulas adopted by these two algorithms are generally different. In this paper, these two algorithms are compared in multi-target detection.

The rest of this paper is organized as follows. In Section 2, the imaging methodologies and basic theories of TR-MUSIC and BP algorithms are introduced. Section 3 compares the two methods in multi-target detection by using the numerical experiment. The conclusion of this paper is presented in Section 4.

2. BASIC THEORY

We consider an array of N transceiver elements whose nth element is located at r_n $(1 \leq n \leq N)$ and the backscattered signals are measured by all elements. Assume that the transceiver elements are all ideal that is the nonlinear of the transceivers can be neglected and targets are taken to be ideal point-like scatterers whose scattering only happens in first order, the receivers in the TRFP stage act as transmitters in the TRBP stage. The number of targets is L and the lth target is located at r_l $(1 \leq l \leq L)$. The incident field at r excited by the emission signal of the nth transmitter denoted by $\varphi_n(r, \omega)$ is

$$\varphi_n(r, \omega) = G(r, r_n, \omega) S_n(\omega) \tag{1}$$

And receiving signal at the mth receiver located at r_m $(1 \leq m \leq N)$ is

$$\psi_{mn}(r, \omega) = \varphi_n(r, \omega) A_r(\omega) G(r_m, r, \omega) = G(r, r_n, \omega) G(r_m, r, \omega) A_r(\omega) S_n(\omega) \tag{2}$$

where $S_n(\omega)$ is the transmission signal of nth transmitter, $A_r(\omega)$ is the scattering factor at r, $G(r_k, r_q, \omega)$ is background Green function that satisfies the reduced wave equation [6], representing the propagator from location r_q to r_k, because of the reciprocity of background Green function, that is $G(r_k, r_q, \omega) = G(r_q, r_k, \omega)$, the expression (2) can be presented as

$$\psi_{mn}(r, \omega) = G(r_n, r, \omega) G(r_m, r, \omega) A_r(\omega) S_n(\omega) \tag{3}$$

2.1. TR-MUSIC

Assume each transmitter individually is excited. So after scattered by L targets, the receiving signal of mth receiver is

$$\psi_m(r,\omega) = \sum_{n=1}^{N}\sum_{l=1}^{L} G(r_n, r_l, \omega) G(r_m, r_l, \omega) \tau_l(\omega) S_n(\omega) \tag{4}$$

where $\tau_l(\omega)$ is the scattering coefficient of lth scatterer.

The time reversal operator $\bar{U}$ can be formed with the multi-static response transfer matrix $\bar{K}$ that incorporates the scattering property of each target and the attenuation in the medium, $\bar{U}$ is given by

$$\bar{U} = \bar{K}^* \bar{K} \tag{5}$$

where the "$*$" denotes the conjugation of a matrix or vector, the multi-static response transfer matrix $\bar{K}$ is

$$\bar{K} = \sum_{l=1}^{L} \bar{G}_l(\omega) \bar{G}_l^T(\omega) \tau_l(\omega) \tag{6}$$

where the superscript "T" denotes the transpose of a vector or matrix, and $\bar{G}_l(\omega)$ is a N-dimensional column vector of Greens function, and can be represented as

$$\bar{G}_l(\omega) = [G(r_1, r_l, \omega), G(r_2, r_l, \omega), \ldots, G(r_N, r_l, \omega)]^T \tag{7}$$

We can obtain the signal and noise sub-spaces by applying eigen decomposition on $\bar{U}$ given by (5). The eigenvalues and eigenvectors of $\bar{U}$ are denoted by $\{\lambda_l, \mu_l\}$ ($l = 1, 2, \ldots, N$). The nonzero eigenvalues correspond to the signal sub-spaces, while the zero eigenvalues correspond to the noise sub-spaces which we use to construct the imaging function. The locations of the targets and their images can be determined by constructing the MUSIC pseudo spectrum from

$$I(r_p) = \frac{1}{\sum\limits_{l_0=L+1}^{N} |\langle \mu_{l_0}^*, \bar{G}_p(\omega)\rangle|^2} \tag{8}$$

where $\mu_{l_0}^*$ is the conjugation of eigenvectors with zero eigenvalues and the inner product $\langle \mu_{l_0}^*, \bar{G}_p(\omega)\rangle$ is equal to zero whenever r_p corresponds to the location of one of the targets.

2.2. BP

To implement the numerical studies, supposing that the imaging region is divided into Q grids. If the nth transmitter is excited and the scatter signal is received by the mth receiver, the scatter field can be represented as

$$E^{scatter}(r_m, r_n, \omega) = \sum_{q=1}^{Q} \psi_{mn}(r_q, \omega) \tag{9}$$

If all transmitters are excited at the same time, the scattered field is given by

$$E^{scatter}(r_m, \omega) = \sum_{n=1}^{N} E^{scatter}(r_m, r_n, \omega) = \sum_{n=1}^{N}\sum_{q=1}^{Q} \psi_{mn}(r_q, \omega) \tag{10}$$

The imaging function of the BP method is

$$I^{BP}(r_p) = \sum_{m=1}^{N} E^{scatter}(r_m, t_{mp}) \tag{11}$$

where $t_{mp} = d_{mp}/c$, c is the light velocity in the free space, d_{mp} is the distance between the mth receiver and the pth grid in the imaging region. $E^{scatter}(r_m, t)$ is the inverse Fourier transform of (10), that is

$$\begin{aligned}E^{scatter}(r_m,t) &= \frac{1}{2\pi}\int_{-\infty}^{+\infty} E^{scatter}(r_m,\omega)e^{j\omega t}d\omega = \frac{1}{2\pi}\sum_{n=1}^{N}\int_{-\infty}^{+\infty} E^{scatter}(r_m,r_n,\omega)e^{j\omega t}d\omega \\ &= \frac{1}{2\pi}\sum_{n=1}^{N}\sum_{q=1}^{Q}\int_{-\infty}^{+\infty}\psi_{mn}(r_q,\omega)e^{j\omega t}d\omega \\ &= \frac{1}{2\pi}\sum_{n=1}^{N}\sum_{q=1}^{Q}\int_{-\infty}^{+\infty}[G(r_n,r_q,\omega)G(r_m,r_q,\omega)A_{r_q}(\omega)S_n(\omega)]e^{j\omega t}d\omega \end{aligned}\tag{12}$$

The discretized version of (12) gives

$$E^{scatter}(r_m,t) = \frac{\Delta\omega}{2\pi}\sum_{k=1}^{K}\left\{\sum_{n=1}^{N}\sum_{q=1}^{Q}[G(r_n,r_q,\omega_k)G(r_m,r_q,\omega_k)A_{r_q}(\omega_k)S_n(\omega_k)]e^{j\omega_k t}\right\}\tag{13}$$

Then, (11) can be written as

$$\begin{aligned}I^{BP}(r_p) &= \sum_{m=1}^{N} E^{scatter}(r_m,t_{mp}) \\ &= \frac{\Delta\omega}{2\pi}\sum_{k=1}^{K}\left\{\sum_{m=1}^{N}\sum_{n=1}^{N}\sum_{q=1}^{Q}\left[G(r_n,r_q,\omega_k)G(r_m,r_q,\omega_k)A_{r_q}(\omega_k)S_n(\omega_k)\right]e^{j\omega_k t_{mp}}\right\}\end{aligned}\tag{14}$$

Which can be formed as

$$\overline{I^{BP}} = \overline{I^{BP}_{Q\times K}}\cdot\bar{Z}\tag{15}$$

where $\bar{Z} = (\frac{\Delta\omega}{2\pi})[1,1,\ldots,1]^T_{1\times K}$. The k^{th} column of matrix $\overline{I^{BP}_{Q\times K}}$ is

$$\overline{I^{BP}_{\omega_k}} = \overline{Ge}(\omega_k)\overline{GA}(\omega_k)\bar{S}(\omega_k)\tag{16}$$

where

$$\bar{Ge}(\omega_k) = \begin{bmatrix}\langle\bar{e}_1(\omega_k),\bar{G}_1(\omega_k)\rangle & \langle\bar{e}_1(\omega_k),\bar{G}_2(\omega_k)\rangle & \ldots & \langle\bar{e}_1(\omega_k),\bar{G}_Q(\omega_k)\rangle \\ \langle\bar{e}_2(\omega_k),\bar{G}_1(\omega_k)\rangle & \langle\bar{e}_2(\omega_k),\bar{G}_2(\omega_k)\rangle & \ldots & \langle\bar{e}_2(\omega_k),\bar{G}_Q(\omega_k)\rangle \\ \vdots & \ldots & \ldots & \vdots \\ \langle\bar{e}_Q(\omega_k),\bar{G}_1(\omega_k)\rangle & \langle\bar{e}_Q(\omega_k),\bar{G}_2(\omega_k)\rangle & \ldots & \langle\bar{e}_Q(\omega_k),\bar{G}_Q(\omega_k)\rangle\end{bmatrix}\tag{17}$$

$$\bar{G}_q(\omega_k) = [G(r_1,r_q,\omega_k),G(r_2,r_q,\omega_k),\ldots,G(r_N,r_q,\omega_k)]^T,\quad (1\le q\le Q)\tag{18}$$

$$\bar{e}_q(\omega_k) = \left[e^{j\omega_k t_{1q}},e^{j\omega_k t_{2q}},\ldots,e^{j\omega_k t_{Nq}}\right]^T,\quad (1\le q\le Q)\tag{19}$$

$$\bar{GA}(\omega_k) = \begin{bmatrix}G(r_1,r_1,\omega_k)A_{r_1}(\omega_k) & G(r_2,r_1,\omega_k)A_{r_1}(\omega_k) & \ldots & G(r_N,r_1,\omega_k)A_{r_1}(\omega_k) \\ G(r_1,r_2,\omega_k)A_{r_2}(\omega_k) & G(r_2,r_2,\omega_k)A_{r_2}(\omega_k) & \ldots & G(r_N,r_2,\omega_k)A_{r_2}(\omega_k) \\ \vdots & \ldots & \ldots & \vdots \\ G(r_1,r_Q,\omega_k)A_{r_Q}(\omega_k) & G(r_2,r_Q,\omega_k)A_{r_Q}(\omega_k) & \ldots & G(r_N,r_Q,\omega_k)A_{r_Q}(\omega_k)\end{bmatrix}\tag{20}$$

$$\bar{S}(\omega_k) = [S_1(\omega_k),S_2(\omega_k),\ldots,S_N(\omega_k)]^T\tag{21}$$

3. NUMERICAL SIMULATIONS

In order to illustrate the performance of these two algorithms in detail, the numerical experiment for three ideal point-like targets is constructed, and two situations are analyzed, that is, target detection with enough transceiver elements called situation I and target detection with few transceiver elements named situation II.

The setup of situation I is conducted as shown in Figure 1, and the setup of situation II is the same as that of situation I except the number of transceiver elements which are shown in the bottom of imaging region in Figure 1. The "△" represents the transceiver element and the "○" represents the target. The positions of these three targets are (1.5 m, 4 m) marked as S_1, (3.75 m, 1.3 m) marked as S_2 and (2.9 m, 2.5 m) marked as S_3. Fifteen transceiver elements are used to construct situation I which provide enough echo signals, for contrast, four transceiver elements are employed to achieve situation II.

The imaging results of TR-MUSIC and BP algorithms are shown in Figure 2 and Figure 3, respectively. In situation I, the targets based on both algorithms can be located accurately, while

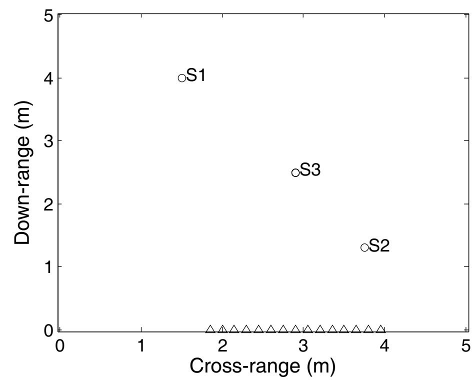

Figure 1: Setup of the numerical experiment.

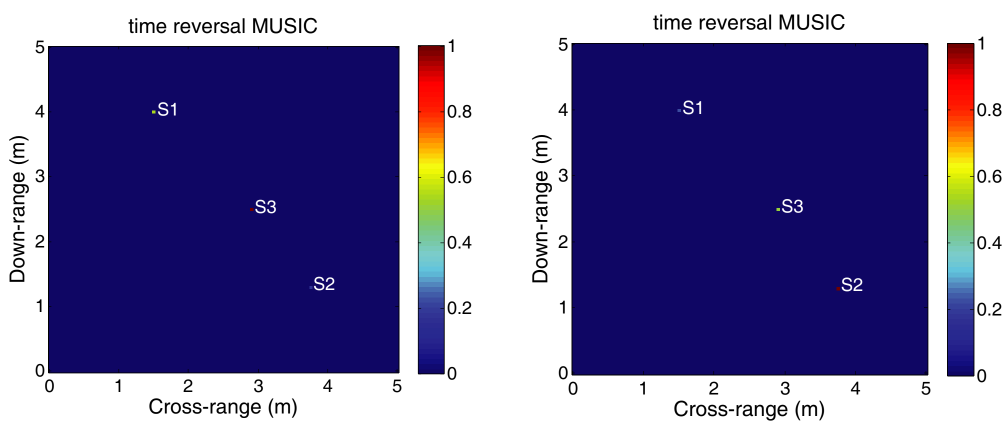

(a) (b)

Figure 2: Imaging results based on TR-MUSIC algorithm: (a) 15 transceiver elements; and (b) 4 transceiver elements.

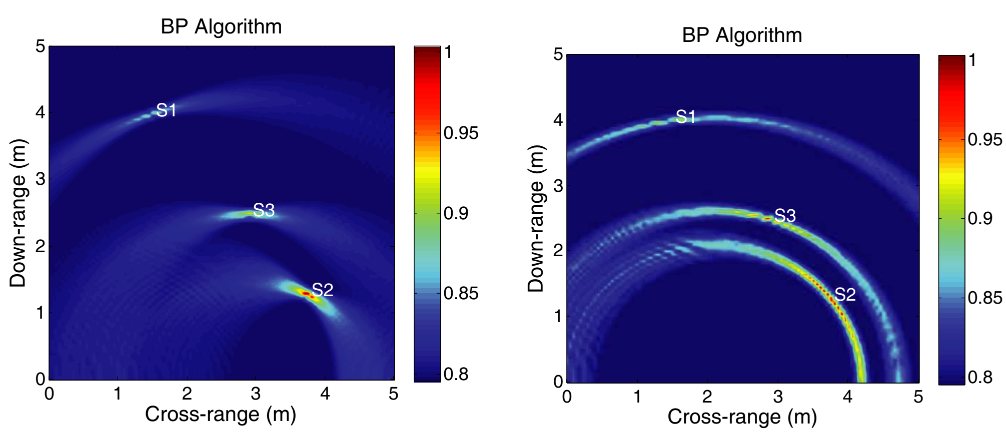

(a) (b)

Figure 3: Imaging results based on BP algorithm: (a) 15 transceiver elements; and (b) 4 transceiver elements.

the imaging resolution based on TR-MUSIC algorithm is better than that based on BP algorithm in situation II. Thus, the TR-MUSIC approach outperforms BP approach in multi-target detection.

4. CONCLUSIONS

Two imaging methods, namely, TR-MUSIC and BP methods have been compared with numerical experiment in multi-target detection. From the analysis, in terms of imaging quality, the TR-MUSIC is superior to the BP method. In our future work, the limitations by using TR-MUSIC will be studied based on some current literature [8], the impact of noise and other impact factors of imaging resolution will be also investigated.

ACKNOWLEDGMENT

This work was supported by the NSFC-Guangdong under Grant No. U1035002, Guangdong-Hong Kong Key Project of Science and Technology under Grant Nos. 2011A011305001 and 2011A0113020 01, and University- Industry Key Project of Department of Education of Guangdong Province under Grant No. CGZHZD1102.

REFERENCES

1. Labyed, Y. and L. J. Huang, "TR-MUSIC inversion of the density and compressibility contrasts of point scatterers," *IEEE Transactions on Ultrasonics, Ferroelectrics and Frequency Control*, Vol. 61, No. 1, 16–24, 2014.
2. Zhang, L., H. L. Li, et al., "Integrating autofocus techniques with fast factorized back-projection for high-resolution spotlight SAR imaging," *IEEE Geoscience and Remote Sensing Letters*, Vol. 10, No. 6, 1394–1398, 2013.
3. Demirci, S., H. Cetinkaya, E. Yigit, C. Ozdemir, and A. A. Vertiy, "A study on millimeter-wave imaging of concealed objects: Application using back-projection algorithm," *Progress In Electromagnetics Research*, Vol. 128, 457–477, 2012.
4. Zhang, W., A. Hoorfar, and L. Li, "Through-the-wall target localization with time reversal MUSIC method," *Progress In Electromagnetics Research*, Vol. 106, 75–89, 2010.
5. Mohan, A. S., M. D. Hossain, and M. J. Abedin, "Beamspace based time reversal processing for breast cancer detection," *IEEE 2012 Antennas and Propagation Society International Symposium*, 1–2, 2012.
6. Brocea, I., G. Papanicolaou, and C. Tsogka, "Theory and applications of time reversal and interferometric imaging," *Inverse Problems*, Vol. 19, No. 6, S139–S164, 2003.
7. Anastasio, M. A., X. C. Pan, and E. Clarkson, "Comments on the filtered backprojection algorithm, range conditions, and the pseudoinverse solution," *IEEE Transactions on Medical Imaging*, Vol. 20, No. 6, 539–542, 2001.
8. Solimene, R. and A. Dell'Aversano, "Some remarks on time-reversal MUSIC for two-dimensional thin PEC scatterers," *IEEE Geoscience and Remote Sensing Letters*, Vol. 11, No. 6, 1163–1167, 2014.